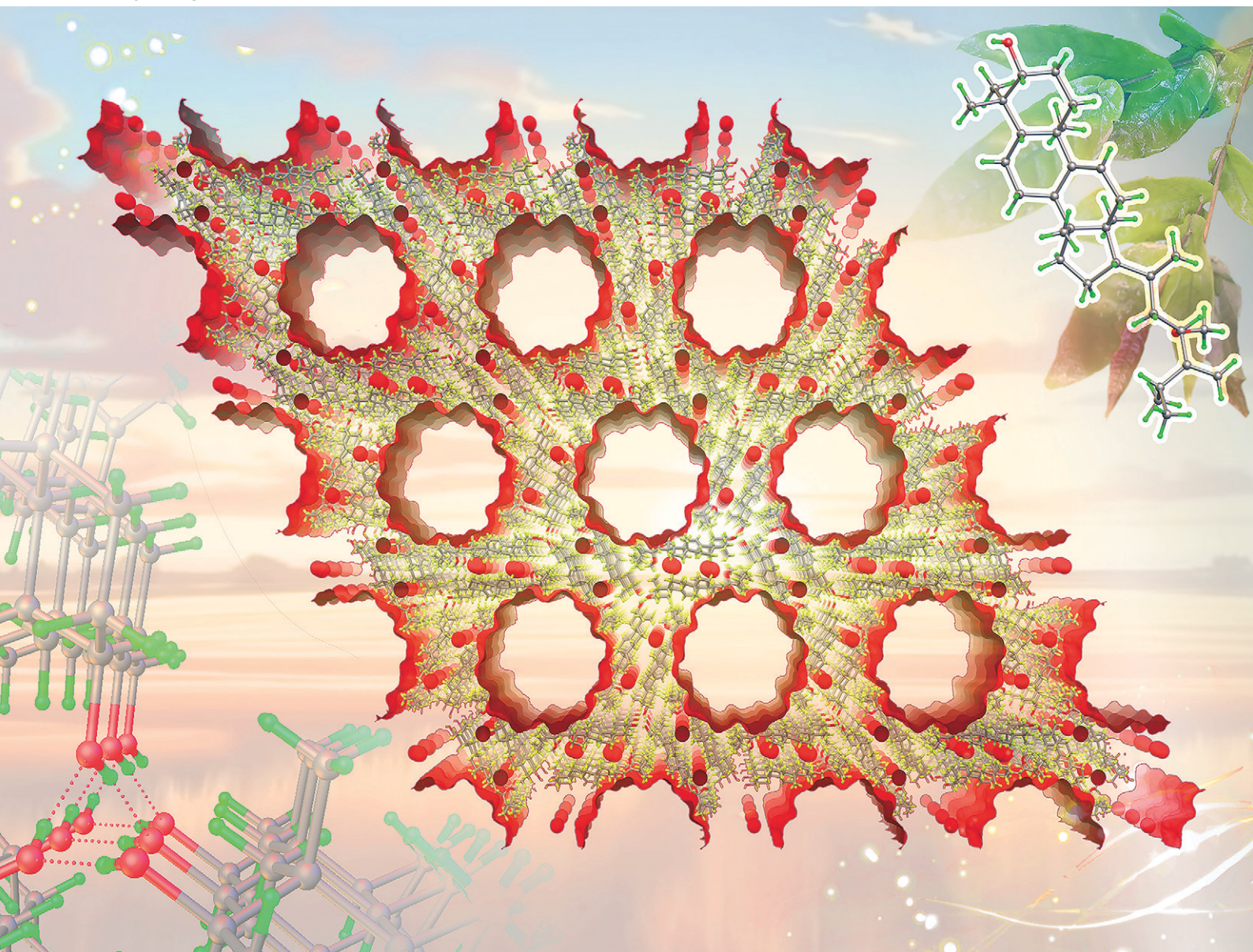


CrystEngComm

rsc.li/crystengcomm



ISSN 1466-8033



Cite this: *CrystEngComm*, 2025, 27, 297

Received 3rd October 2024,
Accepted 19th November 2024

DOI: 10.1039/d4ce01008f

rsc.li/crystengcomm

Structure features of a supramolecular organic framework self-assembled from a chiral natural compound†

Kenika Khotchasanthong,^{id} ^{ab} Yupa Pootaeng-On,^{id} ^c Kanok-on Rayanil,^{id} ^{*c} Mongkol Sukwattanasinitt,^{id} ^d Sakchai Laksee^{id} ^e and Kittipong Chainok^{id} ^{*af}

We present an intriguing instance of a supramolecular-organic framework (SOF) self-assembling from a chiral naturally occurring lanostane compound extracted from the Thai plant *Milium sessilis*. Intermolecular hydrogen bonding and van der Waals forces among molecules form a kinetically stable 3D supramolecular architecture with 1D hollow chiral nanotubes, while Hirshfeld surface analysis provides a visual assessment of these interactions.

Supramolecular organic frameworks (SOFs) are an exciting class of crystalline porous molecular materials that are currently garnering research in the fields of materials science and chemical crystallography.¹ SOFs are assembled by the organization of pure organic or metal-containing organic molecules utilizing a fundamental bottom-up approach *via* noncovalent interactions like hydrogen bonds, halogen bonds, $\pi\cdots\pi$ stacking, and other dispersion forces.² Rather than relying on the robust dative and covalent bonds found in a related class of framework materials such as metal-

organic frameworks (MOFs) and covalent-organic frameworks (COFs), SOF materials provide various advantages including solubility in a variety of solutions, simple regeneration through recrystallization, and synthetic modifiability under mild reaction conditions.³ These benefits arise from the solubility of molecular tectons and the inherent flexibility of weak intermolecular interactions. Moreover, the functionalization of organic molecular tectons in the formation of tailored porous SOFs can improve their stability and adsorption or selectivity abilities.⁴ However, controlling intermolecular interactions that govern molecular arrangement in supramolecular networks while precisely predicting the porosity of the resulting structures remains an uphill experimental challenge. This requires both an understanding of structural modularity into the design of porous SOFs and a detailed comprehension of the mechanisms driving molecular tecton self-recognition.

In the co-crystals of stable supramolecular frameworks, classical robust and directed N/O–H \cdots N/O hydrogen bonds are usually employed as a reliable synthon.⁵ In this context, hetero-aromatic compounds containing nitrogen and/or oxygen atoms, such as amino-triazine and carboxylic acids, can be engineered to yield self-complementary hydrogen-bonded motifs in novel porous SOF crystals.⁶ Weaker C–H \cdots X interactions are crucial in organic solid-state chemistry,⁷ nonetheless, their unpredictable nature present considerable challenges in crystal engineering. The insufficient strength of weaker intermolecular interactions in SOFs, especially at low skeletal densities, frequently affects framework stability and the retention of permanent porosities. This may result in the collapse and/or reorganization of SOFs during the desolvation process.⁸

The majority of structurally established and functionally studied SOFs are synthetic materials made from predesigned organic building molecules. Likewise, MOFs and COFs represent a class of chemically synthesized porous hybrid frameworks. Zeolites, on the other hand, are both synthetic and naturally occurring framework materials consisting of

^a Thammasat University Research Unit in Multifunctional Crystalline Materials and Applications (TU-MCMA), Faculty of Science and Technology, Thammasat University, Pathum Thani 12121, Thailand. E-mail: kc@tu.ac.th

^b Department of Chemistry, Faculty of Science and Technology, Thammasat University, Pathum Thani 12121, Thailand

^c Department of Chemistry, Faculty of Science, Silpakorn University, Nakhon Pathom 73000, Thailand. E-mail: Rayanil_k@su.ac.th

^d Department of Chemistry, Faculty of Science, Chulalongkorn University, Bangkok 10330, Thailand

^e Nuclear Technology Research and Development Center, Thailand Institute of Nuclear Technology (Public Organization), Nakhon Nayok, 26120, Thailand

^f Center of Excellence on Petrochemical and Materials Technology, Chulalongkorn University, Bangkok 10330, Thailand

† Electronic supplementary information (ESI) available: Crystal data for SOF-1 C₃₂H₅₄O₂, *M* = 470.75, colourless block, hexagonal, space group *P*6₄, *a* = 32.3290(19) Å, *c* = 7.1254(5) Å, *V* = 6449.5(9) Å³, *Z* = 6, *T* = 298(2) K, 41 699 reflections collected, 7994 unique (*R*_{int} = 0.079). Final GooF = 0.98, *R*₁ = 0.043, *wR*₂ = 0.105, *R* indices based on 5994 reflections with *I* > 2 σ (*I*) (*F*²), 422 parameters, 307 restraints, μ = 0.05 mm⁻¹. Flack parameter = -0.8(15). CCDC reference number 2366741. For ESI and crystallographic data in CIF or other electronic format see DOI: <https://doi.org/10.1039/d4ce01008f>

various metals and minerals. In this context, we report an interesting instance of a novel SOF material that self-assembles from naturally occurring lanostane triterpene molecules. This compound extracted from the leaves of the traditional Thai plant *Milium sessilis* (Bai-Biaw-Dam-Kwan) found in the southern forests of Thailand. The preliminary investigation employing (^1H , ^{13}C) NMR and HRESIMS indicated the chemical formula $\text{C}_{32}\text{H}_{54}\text{O}_2$ (hereafter named **SOF-1**). The solid-state molecular conformation of **SOF-1** is then established using single crystal X-ray diffraction (XRD).

Single crystals suitable for XRD analysis were obtained by recrystallizing the crude product in a 1:10 (v:v) mixture consisting of ethyl acetate and hexane *via* slow evaporation at room temperature. The phase purity of the bulk **SOF-1** sample was confirmed by experimental powder XRD, showing identical peaks between the as-synthesized sample and the simulated data from the single crystal XRD (Fig. S1 \dagger). According to single crystal XRD analysis, **SOF-1** crystallizes in the hexagonal system with the chiral space group $P6_4$. The absolute configurations of the chiral atoms C2, C5, C6, C9, C13, C14, C17, C23, and C26 are designated as *R*, *R*, *R*, *S*, *S*, *R*, *S*, *S*, and *S*, respectively. Fig. 1 shows the molecular structure of **SOF-1**, which consists of three six-membered (labeled as A, B, and C) and one five-membered (labeled as D) fused rings. All carbon atoms in these rings are sp^3 -hybridized (C–C = 1.490(3)–1.572(3) Å), except for atoms C10 and C11, which are sp^2 -hybridized and possess a double bond [C10=C11 = 1.347(3) Å]. The cyclohexane rings A (C1–C6) and B (C5–C10) both exhibit a chair conformation (the puckering parameters:⁹ $\bar{O}_T = 0.550(3)$ Å, $\theta = 174.7(3)^\circ$, $\omega = 276(3)^\circ$ for ring A, and $\bar{O}_T = 0.552(3)$ Å, $\theta = 13.5(3)^\circ$, $\omega = 91.8(14)^\circ$ for ring B). Meanwhile, the cyclohexene ring C adopts a half-chair conformation [$\bar{O}_T = 0.552(3)$ Å, $\theta = 127.6(3)^\circ$, $\omega = 87.2(5)^\circ$], likely to minimize steric hindrance between the methyl groups. The cyclopentane fragment of ring D exhibits an envelope shape [$\bar{O}_2 = 0.552(3)$ Å, $\omega_2 = 87.2(5)^\circ$], with the C13 atom functioning as the flap. The 4-methoxy-2-methyl-3-methyleneheptane side chain (attached to C17) is equatorially positioned, and exhibits disorder in two positions (0.32:0.68). Notably, the geometric

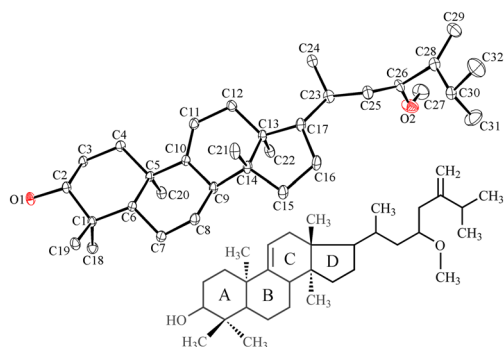


Fig. 1 The chemical structure (bottom) and ORTEP¹¹ plot (top) with the atom-labelling scheme and 25% thermal ellipsoids (hydrogen bond omitted for clarity) of **SOF-1**. The rings in the chemical structure are identified in following discussion using the A–D labelling scheme.

characteristics of the core fused rings are typical and consistent with those of related compounds.¹⁰

The crystal packing showed that the three symmetry-related molecular tectons are arranged in a head-to-head configuration through O–H \cdots O hydrogen bonding ($\text{O1}\cdots\text{O1}^{(i)} = 2.810(1)$ Å, $\angle\text{O1–H1}\cdots\text{O1}^{(i)} = 175$; symmetry code: $(i) -x + y, -x + 1, z - 1/3$) among the hydroxy groups, resulting in a 1D supramolecular chain along the *c* axis as shown in Fig. 2(a). These chains are arranged by two-fold rotational symmetry and interconnected through weak C–H \cdots O hydrogen bonds ($\text{C19}\cdots\text{O1}^{(i)} = 3.416(3)$ Å, $\angle\text{C19–H19}\cdots\text{O1}^{(i)} = 136$; symmetry code: $(i) -x + y, -x + 1, z - 1/3$) involving the methyl and methoxy groups, and further reinforced by weak van der Waals (vdW) forces in a head-to-tail manner (Fig. S2 \dagger). This

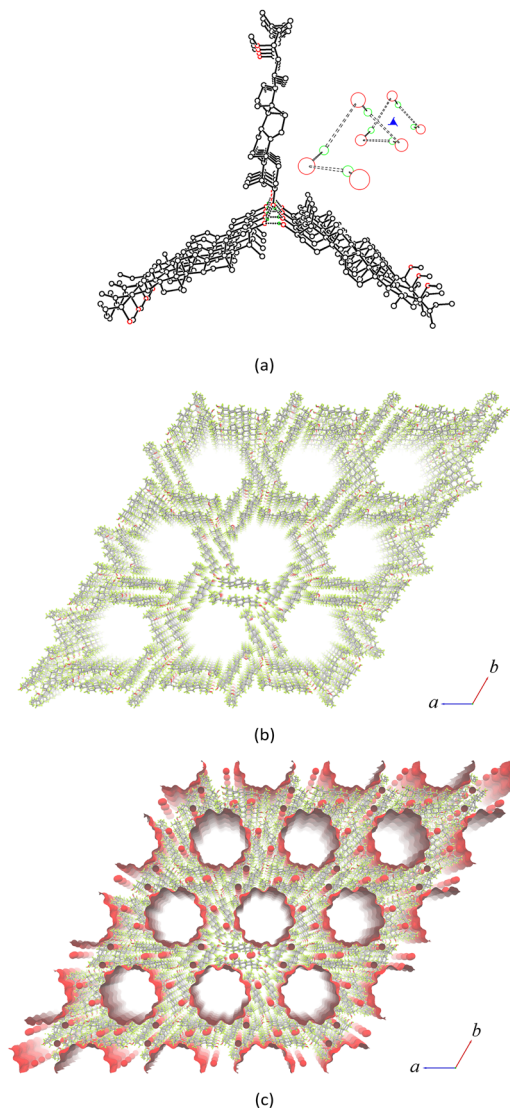


Fig. 2 (a) A classical O–H \cdots O hydrogen-bonded chain aligned parallel to the *c*-axis (only the hydrogen atoms participating in hydrogen bonds are illustrated), (b) bond and stick model showing 3D supramolecular arrangement in the *ab* plane, and (c) the contact surface contours defining the nanochannels (calculated in Mercury¹⁵ using a probe radius of 1.2 Å) of **SOF-1**.

leads to the formation of a 3D supramolecular framework that expands along the *ab* plane as depicted in Fig. 2(b). Indeed, the supramolecular architecture of **SOF-1** is open and contains large 1D hexagonal channels of *ca.* 2.1 nm in diameter centered on the six-fold screw axis. Despite the fact that these tail-to-tail channels are filled with disordered solvent molecules, precise crystallographic solvent modeling is not feasible. Therefore, the SQUEEZE function of the PLATON software suite¹² was utilized to eliminate scattering from the disordered solvent molecules by consolidating voxels located beyond 1.2 Å from the framework. The electron density comprises 36.3% of the total crystal volume (cell volume: 6449.5 Å³, void volume per cell: 2341.0 Å³), Fig. 2(c), indicating that **SOF-1** exhibits significant porosity and may have potential for gas adsorption.

Subsequently, TGA was conducted to assess the thermal stability of the solvated crystals and the structural integrity of the crystals post-solvent removal. Fig. 3 illustrates that the TGA curve of **SOF-1** exhibits a gradual weight loss between 70 and 120 °C, suggesting the loss of solvent molecules. A consistent plateau is observed until 300 °C, after which the structure of **SOF-1** begins to decompose. The desolvated sample of **SOF-1** was also prepared by evacuation at 70 °C for 24 h to evaluate its thermal stability. The thermogram shows no weight loss up to 150 °C, followed by a stable plateau until 300 °C, after which decomposition occurs. It is interesting to note that the PXRD patterns of **SOF-1** and desolvated **SOF-1** exhibit notable differences in the peak position at 2θ (Fig. 3 inset). This implies that the loss of solvent molecules facilitated the structural phase transformation from **SOF-1** to the unidentified desolvated **SOF-1**. The nonporous nature of the desolvated **SOF-1** is further confirmed by the lack of N₂ and CO₂ adsorption (Fig. S3†). This implies the existence of weaker and more flexible intermolecular interactions in **SOF-1** that likely leads to less structural stability. Given that dense structures are thermodynamically favored, external stimuli such as heating the sample under a vacuum would induce kinetically formed open structures to transform into dense structures after the breaking of weak intermolecular interactions, thereby

eliminating their porous features. Thus, the creation of porous SOF materials *via* weak intermolecular interactions is highly complex and presents significant challenges.

Moreover, the Hirshfeld surface analysis¹⁴ generated by the CrystalExplorer software was utilized to visually examine the intermolecular interactions of **SOF-1**. As can be seen in Fig. 4(a) and (b), the d_{norm} surfaces for the asymmetric unit and the six molecular clusters arranged along the *c* axis of **SOF-1** show a bright red region in the upper portion of the surface, which is attributed to the H⋯O/O⋯H contacts. The contacts shown in Fig. 4(c) represent 3.4% of the 2D fingerprint plots, appearing as distinct spikes with $d_e + d_i = 2.30$ Å. This distance is less than the vdW separation sum (2.61 Å)¹⁵ of the two interacting atoms, indicating a short-strong O–H⋯O hydrogen bonding. The blue zone encircling the channels of the assembled six molecular clusters signifies interactions over the vdW sum between the tail chain fragments and the nonpolar solvent molecules. It is evident from Fig. 4(d) that the predominant contributions arise from

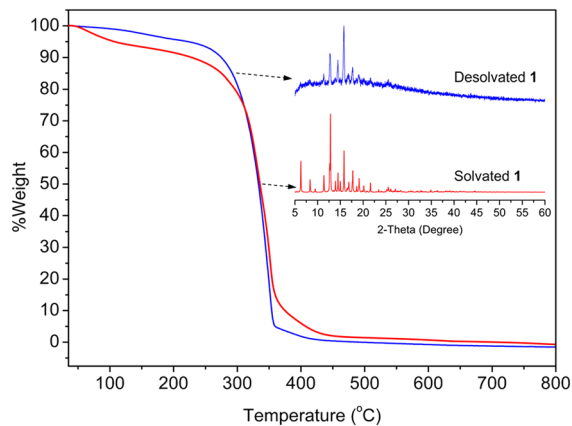


Fig. 3 TGA curves and PXRD patterns (inset) of **SOF-1** and desolvated **SOF-1**.

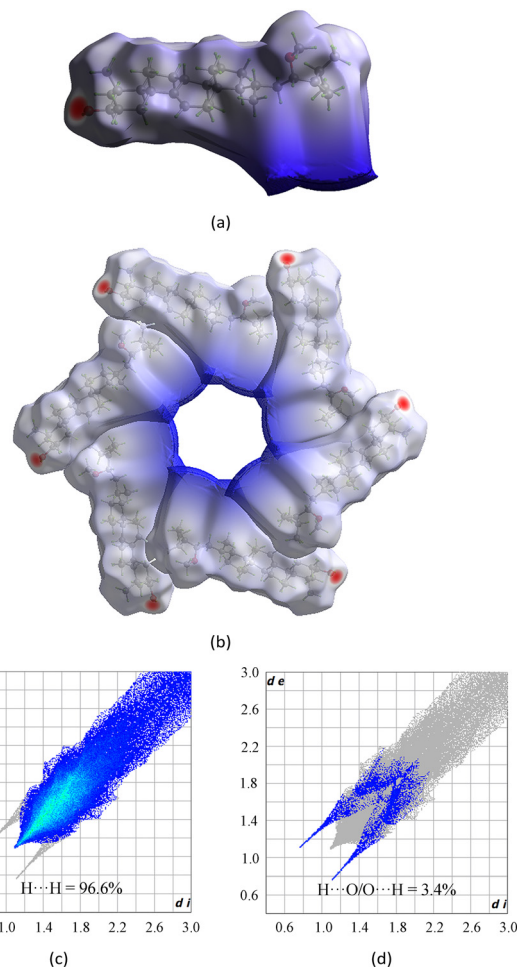


Fig. 4 Hirshfeld surfaces mapped with d_{norm} for (a) the asymmetric unit and (b) the six molecular clusters of **SOF-1**. Intermolecular interactions at the sum of the vdW contacts are highlighted in white, while shorter and longer contacts are represented in red and blue, respectively. Two-dimensional fingerprint plots for the (c) H⋯H and (d) H⋯O/O⋯H contacts of **SOF-1**.

H...H contacts, comprising 96.6%, as can be seen from the characteristic wings in the 2D fingerprint plots with $d_c + d_i \sim 2.20$ Å. This indicates that the vdW forces between molecules have a major impact on the crystal packing arrangement of **SOF-1**. This weak intermolecular force is insufficient to stabilize supramolecular frameworks and establish permanent porosity. Therefore, this may explain the instability observed during the desolvation of **SOF-1**.

Conclusions

We present a noteworthy instance of a supramolecular organic framework (SOF) derived from a naturally occurring compound. The molecular tectons are arranged through hydrogen bonding and reinforced by vdW forces, resulting in a 3D supramolecular architecture having 1D hollow chiral nanotubes with a diameter of 2.1 nm. However, **SOF-1** struggles to stabilize its framework and porous structure after solvent molecule removal, due to weaker intermolecular interactions that diminish the ability to hold molecules efficiently, resulting in poor gas adsorption properties. Nonetheless, the present study shows that the hydroxy group-containing organic skeletons with flexible conformations function as efficient molecular tectons for the synthesis of kinetically stable SOF products. This may aid in the development of novel chiral molecular tectons for exploring the potential of lightweight smart supramolecular frameworks in drug delivery, molecular adsorption, recognition, resolution, and biological applications.

Data availability

Crystallographic data for compound **SOF-1** has been deposited in the Cambridge Crystallographic Data Centre (CCDC). CCDC Number 2366741. The data supporting this article have been included as part of the ESI.†

Author contributions

KK: formal analysis and writing – original draft; YP: investigation and analysis; KR: funding acquisition and writing – review and editing; MK: funding acquisition and supervision; SL: investigation and analysis; KC: conceptualization, funding acquisition, and writing – review and editing.

Conflicts of interest

There are no conflicts to declare.

Acknowledgements

This research was mainly funded by the Thammasat University Research Fund (TUFT-FF1/2565). Additional financial support by the National Research Council of Thailand (NRCT5-RSA63010-01 and N42A661000), the Thailand Institute of Nuclear Technology through their TINT to University programme, and the TU-McMa. K. R. wishes to

acknowledge financial support from the Faculty of Science, Silpakorn University (grant number SRIF-JRG-2567-13). K. K. expresses gratitude for the financing received from the Research and Researchers for Industries funds in Thailand (contact number N41A640263). K. C. expresses gratitude for the support received from the Hub of Talent: Sustainable Materials for Circular Economy, NRCT.

Notes and references

- (a) B. Wang, R.-B. Lin, Z. Zhang, S. Xiang and B. Chen, *J. Am. Chem. Soc.*, 2020, **142**, 14399–14416; (b) Y. Shi, S. Wang, W. Tao, J. Guo, S. Xie, Y. Ding, G. Xu, C. Chen, X. Sun, Z. Zhang, Z. He, P. Wei and B. Z. Tang, *Nat. Commun.*, 2022, **13**, 1882; (c) Y. Guo, C. Wang, G. Mo, Y. Wang, X. Song and P. Li, *Cryst. Growth Des.*, 2023, **23**, 7635–7646; (d) T. Hashimoto, R. Oketani, M. Nobuoka and S. Seki, *Angew. Chem., Int. Ed.*, 2023, **62**, e202215836; (e) X.-J. Xi, Y. Li, F. Lang, J. Pang and X.-H. Bu, *Chem. Sci.*, 2024, **15**, 4529–4537.
- (a) I. Hisaki, C. Xin, K. Takahashi and T. Nakamura, *Angew. Chem., Int. Ed.*, 2019, **58**, 11160–11170; (b) P. Li, M. R. Ryder and J. F. Stoddart, *Acc. Mater. Res.*, 2020, **1**, 77–87; (c) Z.-T. Li, S.-B. Yu, Y. Liu, J. Tian and D.-W. Zhang, *Acc. Chem. Res.*, 2022, **55**, 2316–2325; (d) T. Vijayakanth, S. Dasgupta, P. Ganatra, S. Rencus-Lazar, A. V. Desai, S. Nandi, R. Jain, S. Bera, A. I. Nguyen, E. Gazit and R. Misra, *Chem. Soc. Rev.*, 2024, **53**, 3640–3655; (e) F. Frezza, A. Matěj, A. Sánchez-Grande, M. Carrera, P. Mutombo, M. Kumar, D. Curiel and P. Jelínek, *J. Am. Chem. Soc.*, 2024, **146**, 3531–3538.
- (a) J. Li and B. Chen, *Chem. Sci.*, 2024, **15**, 9874–9892; (b) S. Hu, H. Zhao, M. Liang, J. Hao and P. Xue, *Chem. Commun.*, 2024, **60**, 8140–8152.
- (a) D.-D. Zhou, Y.-T. Xu, R.-B. Lin, Z.-W. Mo, W.-X. Zhang and J.-P. Zhang, *Chem. Commun.*, 2016, **52**, 4991–4994; (b) W. Yan, X. Yu, T. Yan, D. Wu, E. Ning, Y. Qi, Y.-F. Han and Q. Li, *Chem. Commun.*, 2017, **53**, 3677–3680; (c) Y. Yang, H. Zhang, Z. Yuan, J.-Q. Wang, F. Xiang, L. Chen, F. Wei, S. Xiang, B. Chen and Z. Zhang, *Angew. Chem., Int. Ed.*, 2022, **61**, e202207579; (d) D. W. Kim, Y. Chen, H. Kim, N. Kim, Y. H. Lee, H. Oh, Y. G. Chung and C. S. Hong, *Adv. Mater.*, 2024, **36**, 2401739.
- (a) I. Hisaki, S. Nakagawa, N. Ikenaka, Y. Imamura, M. Katouda, M. Tashiro, H. Tsuchida, T. Ogoshi, H. Sato, N. Tohnai and M. Miyata, *J. Am. Chem. Soc.*, 2016, **138**, 6617–6628; (b) T. Adachi and M. D. Ward, *Acc. Chem. Res.*, 2016, **49**, 2669–2679; (c) M. Morshedi, J. S. Ward, P. E. Kruger and N. G. White, *Dalton Trans.*, 2018, **47**, 783–790; (d) M. Mastalerz and I. M. Oppel, *Angew. Chem., Int. Ed.*, 2012, **51**, 5252–5255; (e) J. Yang, J. Wang, B. Hou, X. Huang, T. Wang, Y. Bao and H. Hao, *Chem. Eng. J.*, 2020, **399**, 125873; (f) Z.-J. Lin, S. A. R. Mahammed, T.-F. Liu and R. Cao, *ACS Cent. Sci.*, 2022, **8**, 1589–1608.
- (a) S. Horike, S. Shimomura and S. Kitagawa, *Nat. Chem.*, 2009, **1**, 695–704; (b) J. Lü, C. Perez-Krap, M. Suyetin, N. H. Alsmail, Y. Yan, S. Yang, W. Lewis, E. Bichoutskaia, C. C. Tang, A. J. Blake, R. Cao and M. Schröder, *J. Am. Chem. Soc.*,

- 2014, **136**, 12828–12831; (c) Q. Huang, W. Li, Z. Mao, L. Qu, Y. Li, H. Zhang, T. Yu, Z. Yang, J. Zhao, Y. Zhang, M. P. Aldred and Z. Chi, *Nat. Commun.*, 2019, **10**, 1–8; (d) J. Liu, Y.-Q. Fan, S.-S. Song, G.-F. Gong, J. Wang, X.-W. Guan, H. Yao, Y.-M. Zhang, T.-B. Wei and Q. Lin, *ACS Sustainable Chem. Eng.*, 2019, **7**(14), 11999–12007; (e) Q. Chen, X. Chen, M. Liang, Y. Han and P. Xue, *CrystEngComm*, 2022, **24**, 2575–2590; (f) M. Zhao, L. Sun, Y. Yang, X.-S. Gu and C.-J.-S. Lai, *Coord. Chem. Rev.*, 2024, **514**, 215881.
- 7 (a) T. Steiner, *J. Phys. Chem. A*, 2000, **104**, 433–435; (b) G. R. Desiraju, *Chem. Commun.*, 2005, 2995–3001; (c) S. Lim, H. Kim, N. Selvapalam, K.-J. Kim, S. J. Cho, G. Seo and K. Kim, *Angew. Chem., Int. Ed.*, 2008, **47**, 3352–3355; (d) J. Bernstein, *Cryst. Growth Des.*, 2013, **13**, 961–964.
- 8 (a) A. Bērziņš, A. Trimdale, A. Kons and D. Zvaniņa, *Cryst. Growth Des.*, 2017, **17**, 5712–5724; (b) I. Hisaki, Y. Suzuki, E. Gomez, Q. Ji and N. Tohnai, *J. Am. Chem. Soc.*, 2019, **141**, 2111–2121; (c) N. Chongboriboon, K. Samakun, T. Inprasit, F. Kielar, W. Dungkaew, L. W.-Y. Wong, H. H.-Y. Sung, D. B. Ninković, S. D. Zarić and K. Chainok, *CrystEngComm*, 2020, **22**, 24–34.
- 9 D. Cremer and J. A. Pople, *J. Am. Chem. Soc.*, 1975, **97**, 1354–1358.
- 10 (a) M. Chikada, K. Sada and M. Miyata, *Polym. J.*, 1999, **11**, 1061–1064; (b) Y.-L. Lin, W.-Y. Wang, Y.-H. Kuo and Y.-H. Liu, *Chem. Pharm. Bull.*, 2001, **49**, 1098–1101; (c) K. Sada, M. Sugahara, K. Kato and M. Miyata, *J. Am. Chem. Soc.*, 2001, **123**, 4386–4392; (d) K. Nakano, E. Mochizuki, N. Yasui, K. Morioka, Y. Yamauchi, N. Kanehisa, Y. Kai, N. Yoswathananont, N. Tohnai, K. Sada and M. Miyata, *Eur. J. Org. Chem.*, 2003, **13**, 2428–2436; (e) M. Miyata, N. Tohnai and I. Hisaki, *Acc. Chem. Res.*, 2007, **40**, 694–702; (f) Y.-L. Li, Y.-X. Gao, H.-Z. Jin, L. Shan, X.-S. Liang, X.-K. Xu, X.-W. Yang, N. Wang, A. Steinmetz, Z. Chen and W.-D. Zhang, *Phytochemistry*, 2014, **106**, 116–123; (g) P. Paileea, T. Kruahong, S. Hongthong, C. Kuhakarn, T. Jaipetch, M. Pohmakotr, S. Jariyawat, K. Suksen, R. Akkarawongsapat, J. Limthongkul, A. Panthong, P. Kongsaree, S. Prabpai, P. Tuchinda and V. Reutrakul, *Phytochem. Lett.*, 2017, **20**, 111–118.
- 11 L. J. Farrugia, *J. Appl. Crystallogr.*, 2012, **45**, 849–854.
- 12 (a) A. L. Spek, PLATON, *Acta Crystallogr., Sect. D: Biol. Crystallogr.*, 2009, **65**, 148–155; (b) A. L. Spek, *J. Appl. Crystallogr.*, 2020, **53**, 226–235.
- 13 C. F. Macrae, I. Sovago, S. J. Cottrell, P. T. A. Galek, P. McCabe, E. Pidcock, M. Platings, G. P. Shields, J. S. Stevens, M. Towler and P. A. Wood, *J. Appl. Crystallogr.*, 2020, **53**, 226–235.
- 14 (a) M. A. Spackman and J. J. McKinnon, *CrystEngComm*, 2002, **4**, 378–392; (b) J. J. McKinnon, D. Jayatilaka and M. A. Spackman, *Chem. Commun.*, 2007, 3814–3816; (c) M. A. Spackman and D. Jayatilaka, *CrystEngComm*, 2009, **11**, 19–32; (d) P. R. Spackman, M. J. Turner, J. J. McKinnon, S. K. Wolff, D. J. Grimwood, D. Jayatilaka and M. A. Spackman, *J. Appl. Crystallogr.*, 2021, **54**, 1006–1011.
- 15 A. Bondi, *J. Phys. Chem.*, 1964, **68**, 441–451.